Direct Kinetics Study of the Reaction of Peroxyacetyl Radical with NO between 218 and 370 K

Tamar Moise, Wolfgang Denzer,† and Yinon Rudich*

Department of Environmental Sciences, Weizmann Institute, Rehovot 76100, Israel

Received: March 12, 1999; In Final Form: July 1, 1999

The rate coefficient of the $CH_3C(O)O_2$ + NO gas-phase reaction was measured over the temperature range of 218−370 K and total pressure of 2−5 Torr, using chemical ionization mass spectrometry detection of the $CH_3C(O)O_2$ radical. The temperature-dependent expression for the rate coefficient was determined to be $k(T) = (6.0 \pm 1.1) \times 10^{-12} \exp\{(320 \pm 40)/T\}$ cm^3 molecule^{-1} s^{-1}, and a 298 K rate constant $k_{298} = (1.8 \pm 0.3) \times 10^{-11}$ cm^3 molecule^{-1} s^{-1} was found. These results quell some of the ambiguity presented by previous studies of this reaction and validate the recommended value to be used in tropospheric chemistry models.

Introduction

Peroxyacetyl radical (PA, $CH_3C(O)O_2$) is a common intermediate in the atmospheric photodegradation process of a vast group of organic species including acetone, acetaldehyde, methylglyoxal, and isoprene. The peroxyacetyl radical reacts mainly with HO_2, other peroxy radicals, and NO_x(=NO_2 and NO). In polluted air, with high NO_x concentrations, the reactions of the PA radical are primarily with NO and NO_2

$$CH_3C(O)O_2 + NO_2 + M \rightleftarrows CH_3C(O)O_2NO_2 + M \quad (1,-1)$$

$$CH_3C(O)O_2 + NO \rightarrow CH_3C(O)O + NO_2 \quad (2)$$

The association reaction of the PA radical with NO_2 (R1) forms peroxyacetyl nitrate (PAN), a relatively stable adduct, providing a mechanism for sequestering and long-range transport of NO_x in the troposphere. In contrast to PAN formation that sequesters NO_2, the reaction of $CH_3C(O)O_2$ with NO converts nitric oxide to NO_2, eventually leading to ozone production after the subsequent photolysis of NO_2 and formation of atomic oxygen. The rate of reaction R2 directly affects the extent of NO_x binding in the reservoir species PAN and determines the fate of the PA radical following thermal decomposition of PAN in NO_x-rich environments. The rate constants of these two reactions are thus important for assessing the photochemical availability of NO_x and for evaluating the role of peroxyacetyl radicals in tropospheric ozone formation.

The PA + NO reaction has been investigated by several groups.[1−7] Indirect studies of the reaction have suggested that reaction R2 is insensitive to temperature.[1−3] Two temperature-dependent direct studies of the absolute rate constant for R2 have recently been undertaken.[4,5] One of the studies determined the rate coefficient using a fast flow tube reactor in conjunction with chemical ionization mass spectrometry (CIMS),[4] whereas the second employed transient IR absorption and time-resolved UV absorption spectroscopy.[5] The two studies differ in the radical concentrations used, the detection technique, and data analysis. Both observed moderate temperature dependence of the reaction. However, they report different values and the room-temperature rate coefficients differ by about 30%. Villalta and Howard[4] report $k_{2(298)} = (2.0 \pm 0.3) \times 10^{-11}$ cm^3 molecule^{-1} s^{-1} and a temperature-dependent rate coefficient of $k_2(T) = (8.1 \pm 1.3) \times 10^{-12} \exp\{(270 \pm 60)/T\}$ cm^3 molecule^{-1} s^{-1}, while Maricq and Szente[5] report $k_{2(298)} = (1.4 \pm 0.2) \times 10^{-11}$ cm^3 molecule^{-1} s^{-1} and a temperature-dependent rate coefficient of $k_2(T) = (2.1^{+1.4}_{-0.8}) \times 10^{-12} \exp\{(570 \pm 140)/T\}$ cm^3 molecule^{-1} s^{-1}. The JPL NASA recommended value[8] based on both studies is $k_2(T) = 5.3 \times 10^{-12} \exp(360/T)$ cm^3 molecule^{-1} s^{-1}, yielding $k_{2(298)} = 1.8 \times 10^{-11}$ cm^3 molecule^{-1} s^{-1}. The most recent study by Sehested et al.[6] using pulse radiolysis at high pressure yields a room-temperature rate constant $k_{2(298)} = (2.0 \pm 0.3) \times 10^{-11}$ cm^3 molecule^{-1} s^{-1}, in good agreement with the results of the flow tube study.[4] However, no temperature dependence was measured in that study.

As discussed above, the ratio of the rate constants k_2/k_1 is an essential value in the atmospheric chemistry of PAN as it determines its lifetime in the troposphere. Recently, two studies have reported direct determination of this ratio at high pressure of SF_6 and CO_2 by probing the relative PAN concentration as a function of the [NO]/[NO_2] ratio.[6,7] The value of this ratio was found to be $k_2/k_1 = 2.1 \pm 0.3$ and does not seem to depend on temperature.[6,7] A proper measurement of reaction R2 over a wide temperature range allows for absolute PA + NO_2 rate constants (k_1) to be obtained using these directly measured ratios.

The two main loss processes for PAN, photolysis and thermal decomposition, have well characterized temperature dependencies.[9−11] This warrants an equally comprehensive understanding of the temperature dependence for the PA + NO and PA + NO_2 reactions in order to assess the role of these reaction pathways following PAN thermal decomposition. We report an additional direct, temperature-dependent measurement for the rate coefficient of the peroxyacetyl + NO reaction which alleviates some of the questions presented by previous studies of this reaction and confines the recommended value to be incorporated into urban and regional tropospheric chemistry models. We also use this measurement to determine the rate coefficient of the PA + NO_2 reaction.

* To whom correspondence should be addressed.
† Current address: Physical & Theoretical Chemistry Laboratory, Oxford University, South Parks Rd., Oxford OX1 QZ, UK.

10.1021/jp990876w CCC: $18.00
Published on Web 08/05/1999

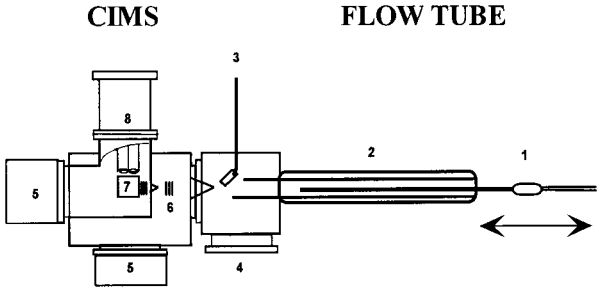

Figure 1. Schematic description of the newly built flow-tube/CIMS system. 1: Movable injector with an oven for PAN thermal decomposition (400−500 K). 2: Temperature regulated glass flow tube. 3: Inlet for SF_6^-/He for ion generation by HV discharge. 4: Pumping port. 5: Turbo molecular pumps. 6: Einzel lens stack and biasable orifice and skimmer for ions extraction. 7: Quadrupole deflector. 8: Quadrupole mass filter.

Experiment

Apparatus and Radical Generation. The experimental technique employed in this study uses a fast-flow reactor coupled to a chemical ionization mass spectrometer (CIMS). The CIMS technique is advantageous as it enables selective ionization of species and causes little fragmentation of the parent molecule. The reagent ion used here was SF_6^-, which reacts by fast charge transfer with the PA radical[4] with a rate coefficient of $k_{(298)} = (7^{+4}_{-2}) \times 10^{-10}$ cm^3 molecule^{-1} s^{-1} to give the ion at $m/e = 75$. A schematic description of the system is shown in Figure 1.

The reaction of PA radicals with NO was studied in a temperature regulated, glass flow tube reactor of 40 cm length and 2.2 cm i.d.. The PA radical flow was introduced into the system through a moveable injector (length 50 cm, 9 mm o.d.). NO was added at a fixed position upstream from the injection point. Kinetic data was obtained by varying the exposure time of the PA radical to NO within the reaction zone, i.e., by changing the injector position.

Peroxyacetyl radicals were generated by the thermal decomposition of PAN in an oven (400−500 K, 14 cm long 20 mm diameter) mounted on the injector.

$$CH_3C(O)O_2NO_2 \xrightarrow{\Delta} CH_3C(O)O_2 + NO_2 \qquad (3)$$

PAN was synthesized according to the procedure of Gaffney et al.[12] and stored in tridecane. The PAN/tridecane solution was kept at 200 K and slightly warmed to a temperature of ca. 215 K during the experiments to minimize the concentration of the PA radicals in the flow tube. A small, ∼1 sccm, He flow (>99.999%) carried PAN vapor to the upper end of the movable injector. Additional He was introduced through the injector and through a separate fixed inlet on the top of the flow tube (∼2000 sccm) to achieve fast flows and minimize self-recombination reactions. All flows were controlled by mass-flow controllers (MKS 247) calibrated periodically using a referenced Gilian Gilbrator flow cell. The temperature and pressure were monitored by a thermocouple and a capacitance pressure transducer (Baratron MKS 722), respectively, halfway along the reaction zone.

SF_6^- reagent ions are produced via a corona discharge of a constantly flowing SF_6/He mixture (SF_6, 1−4 sccm; He, 2000 sccm). The discharge takes place between a stainless steel needle floating at around −2 kV (Fluke 408B) and the surrounding grounded $^1/_4$ in. tubing. The discharge current is limited to ∼70 μA. The corona discharge is positioned in the first chamber of the mass spectrometer, at an angle of 45° with regard to the reactants. This chamber is pumped by a booster pump (Edwards EH500 backed by E2M80). The neutral (reactants and reaction products) and ion beams are combined in this chamber, 4 cm away from a 0.5 mm diameter orifice of a biasable skimmer that extracts the products of the charge-transfer reaction into the second chamber. The SF_6^-/neutral reaction time is approximately 20 μs. To prevent species from the flow tube from entering the high-voltage region, a 4 cm long glass sleeve is placed over the generated plasma. In the second chamber, the ions are focused through an Einzel lens assembly toward a second aperture (∼1 mm). After passing into the third chamber, the ions are deflected by a quadrupole deflector 90° into the quadrupole mass filter (Extrel 150 QC). The neutral flow continues collinear directly into a turbomolecular pump. This configuration minimizes the flow of gas through the mass filter and enhances its performance. The mass spectrometer is pumped by two turbo drag molecular pumps (Varian macro Torr V-250 and V-550) backed by a rotary pump (Varian SD 450). The ion signal is monitored using a counting preamplifier.

Kinetic Measurements. The PA + NO reaction was measured over a temperature range from 218 to 370 K. The flow from the injector equilibrated with the jacket temperature within ∼0.5 cm from its entrance into the flow tube, deviating at most by 0.5 K. Velocity attained was between 1800 and 3200 cm/s, allowing a maximal reaction time of between 16 and 12 ms. The experiments were done at 2−5 Torr.

The kinetic measurements were taken under pseudo-first-order conditions (i.e., $[NO] \gg [CH_3C(O)O_2]$). The reaction thus becomes first order with regard to the radical species, PA, and the rate equation is

$$\frac{d[PA]}{dt} = -k^I[PA] \qquad (4)$$

The first-order rate constant is k^I (s^{-1}) = $k^{II}[NO] + k_w$, where k^{II} is the second-order rate constant (cm^3 molecule^{-1} s^{-1}) for reaction R2, [NO] is the concentration of the added reactant (molecule cm^{-3}), and k_w (s^{-1}) is the first-order rate coefficient for loss of peroxy radicals on the wall of the flow tube. For a pseudo-first order reaction, only the relative concentration of the radical needs to be measured for any reaction point.

The radical $CH_3C(O)O_2^-$ was monitored at its parent mass peak, $m/e = 75$, and its decrease following the reaction with NO was used to monitor the reaction. Care was taken to obtain a nondistorted and symmetric ion peak signal. The PA ion signal was constant to 1−2%. For each injector position, the signal area was measured first for the pure PA flow and then after NO has been added. The ratio between these two signals gives the relative decrease in PA radicals at a certain position. Use of the ratio at each point allowed wall losses and geometrical disturbances that could occur along the reaction path in the course of the measurements to be directly taken into account. The injection of the radicals through the injector allows determination of the actual rate of loss on the reactor wall. This arrangement is different from the previous measurements[4,13−16] in which only the loss on the injector was determined since the PA radical was formed in a fixed sidearm. At room temperature, the PA signal intensity hardly decreases with the movement of the injector, indicating that wall losses in the flow tube play only a minor role in our system. The losses increased with decreasing temperature.

An additional complexity arises due to the time spent by the PA radicals in the injector, since a portion of the radicals recombine or react with NO_2 before the injection to the flow tube. At temperatures different from room temperature, the PA signal varied depending on the portion of the injector that was

in the temperature regulated zone. Therefore, at each injector position, care was taken that the PA signal had equilibrated to the flow tube conditions. Again, the use of signal ratio ensured that the measured changes were due to reaction with NO only. The use of ratios also eliminated complications due to the slight changes in temperature in the noneutectic dry ice/ethanol mixture, causing varying PAN flows from the PAN/tridecane mixture.

The CIMS detection of the PA radical is accomplished by its ionization by a reagent ion, SF_6^-. When a sufficiently small conversion of the reagent ion is maintained, the ion signal at *m/e* 75 is directly proportional to the PA radical concentration in the reactor.[4] To ensure a high SF_6^-/PA concentration ratio, the PAN/tridecane mixture was cooled to a temperature that yielded a PA signal of ca. 150 000 cps. Count rates for the SF_6^- signal were about 1×10^7 cps. The background counts for the PA radical were typically less than 500 cps. Care was taken that the SF_6^- ion signal amplitude remained stable between each measurement.

As the flow tube and the chamber where the plasma is generated were under the same pressure system, pressure variations upon addition of high NO concentrations caused slight changes in the SF_6^- signal. This dictated the upper limit of NO concentrations with which the reaction was studied.

NO was used from a prepared diluted He/NO mixture (<2% NO) stored in a glass bulb. On preparation, NO was passed through a silica gel trap cooled to 200 K to absorb any trace NO_2 and N_2O_4 present in the NO cylinder (99.95% purity). The NO flows were determined by introducing a NO/He mixture of known concentration into a calibrated volume and measuring the pressure change for a given time interval. NO concentrations ranged from 1.5×10^{12} to 10.8×10^{12} molecules cm^{-3}.

PA Concentration and Detection Limit. The concentration of the PA radical in the flow tube was estimated in a number of ways. First, an estimate of the concentration decrease at *m/e* 75 due to reaction R2 was made from the observed increase of the NO_2 signal at *m/e* 46. This calibration method provides an upper limit for the PA concentration, because it assumes that one NO_2 molecule is produced for every $CH_3C(O)O_2$ molecule consumed. To calibrate the NO_2 signal intensity against a known concentration, NO_2 was added to the flow from a calibrated He/NO_2 bulb under typical experimental conditions. These experiments constrain the PA concentration between 4.0×10^{10} and 1.5×10^{11} molecule cm^{-3}. This range was relatively broad due to a peak at *m/e* 66 observed at the time of calibration, which was associated with the NO_2 bulb. The additional mass peak leads to uncertainty in the 1:1 assumption between the depleted and product peaks.

Another estimate for the PA concentration was made by considering ~3% depletion in the PA signal observed after addition of a known NO_2 concentration, presumably due to reaction (R1). This calculation leads again to PA estimates of $\sim 1.5 \times 10^{11}$ molecule cm^{-3}. Considering 1.5×10^{11} molecule cm^{-3} as the average value of the PA radical concentration implies that the detection sensitivity of the system is 2×10^9 molecule/cm^3, calculated by assuming a signal/noise ratio of 10.

Results

Mass Spectra. When the carrier gas passed through the PAN/tridecane reservoir, a signal at *m/e* 46 appeared, accompanied by smaller peaks at *m/e* 59, 62, and 82. These peaks are assigned as NO_2^-, $CH_3C(O)O^-$, NO_3^-, and NO_3^-·HF. No signal was observed at the parent peak mass of PAN (*m/e* 121). On heating

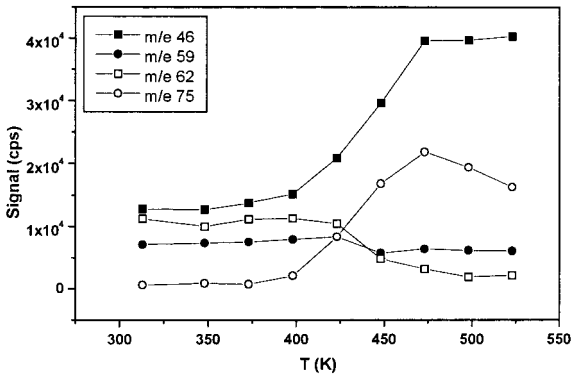

Figure 2. Dissociation of PAN in the oven. The main identified peaks are *m/e* 42, 59, 62, and 75. Experiments were performed at the temperature in which the *m/e* 75 (PA radical) is maximal.

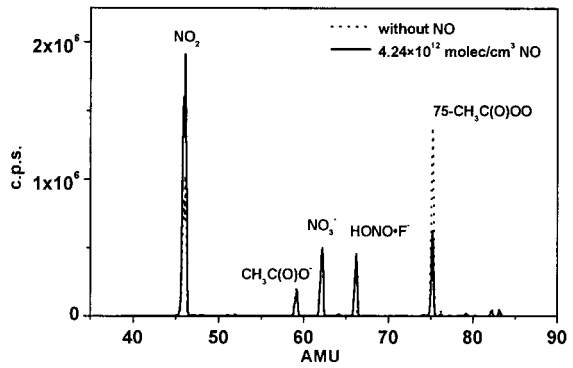

Figure 3. Changes in the mass spectra following addition of NO to the flow tube. The only depleted signal is that of the PA radical (*m/e* 75). The NO_2 peak (*m/e* 46) increases, confirming that NO_2 is a primary product. See discussion for the assignment of *m/e* 66. The count rates in the figure are higher than the ones used during experiments for clarity.

of the quartz oven, the signal of the NO_2^- peak increased. The $CH_3C(O)O_2^-$ signal from the thermal decomposition of PAN (*m/e* 75) appeared at ~430 K. NO_2^- and $CH_3C(O)O_2^-$ became the dominant signals and continued to increase in intensity until the $CH_3C(O)O_2^-$ signal reached a maximum, typically at ~510 K. A decrease in intensity observed at higher temperatures is attributed to self-reactions or thermal decomposition of the PA radical (Figure 2). The signal intensities in the mass spectra differed depending on the PAN reservoir temperature, flow velocities, flow tube pressure, and high-voltage applied to the corona discharge. With all the variability between runs, the peaks at *m/e* = 46 and 75 were always dominant on heating, about an order of magnitude higher than the other peaks. It should be noted that other than the ion signals mentioned above, no significant change was detected in any of the other small peaks associated with the content of the PAN bubbler (<3000 cps) on heating.

As shown in Figure 3, the only signal to be depleted following reaction with NO is that of $CH_3C(O)O_2^-$. This decrease is accompanied by an increase of the NO_2 signal, indicating that NO_2 is a major reaction product of the title reaction. Therefore, reaction R2 was monitored by observing the decrease of the PA radical only.

The other expected products for the reaction are $CH_3C(O)O$, CH_3, and CO_2. Several attempts to detect these products ($CH_3C(O)O$ and CH_3 as methoxy radical and CO_2 using the charge-transfer reactions with SF_6^-, O_2^+, and O_3^-, respectively) were not successful. Villalta et al.[4] could not observe the *m/e* 59 peak as well, and it is widely assumed to decompose directly immediately after formation.[6] The lack of increase of the *m/e*

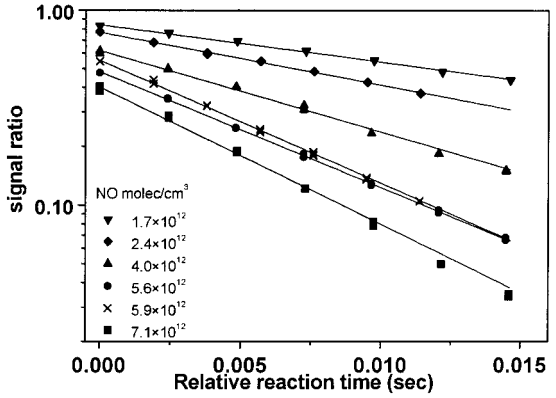

Figure 4. Semilog plots of $CH_3C(O)O_2$ signal vs relative reaction time with NO at $T = 242$ K. Conditions are $v = 2055-2635$ cm s^{-1}, $P = 3.7-4.6$ Torr, and [NO] $= (1.7-7.1) \times 10^{12}$ cm^{-3}.

$= 59$ peak following the reaction suggests that the $CH_3C(O)O$ radical formed by PA + NO reaction is indeed very short-lived and undergoes direct decay into other products, probably $CH_3 + CO_2$. This may be explained by formation of a thermally unstable product, due to the large exothermicity of R2.[8] It is interesting to note also that, in the study of $CH_2{=}C(CH_3)C(O)O_2 + NO$,[17] the only identified product was NO_2. However, CO_2 was detected as a reaction product by Sehested et al.[6]

The smaller peak at mass 66 that arises following the reaction with NO is assigned to either $NO_2^-{\cdot}HF$ or $HONO{\cdot}F^-$. The latter peak may form by the charge-transfer reaction of SF_6^- with HONO that heterogeneously forms on the walls of the injector or flow tube. Another possible assignment for this mass might be the formation of the adduct $CH_3O_2{\cdot}F^-$, which would indicate the dissociation to methyl radical and subsequent reaction with O_2. On addition of excess O_2 to the flow tube, the signal intensity of $m/e = 66$ rose only slightly, the only signal increasing substantially being NO_2. Kinetics simulation of the reaction yields very low CH_3O_2 concentrations, well below the detection limit of the apparatus (see Discussion).

Rate Coefficient. Decay curves of the $CH_3C(O)O_2^-$ signal ratio, with and without NO flow, were plotted vs relative reaction time for each concentration of NO. Typical first-order decay plots for 242 K measurements with different NO concentrations are shown in Figure 4. The slopes of these curves yield the first-order rate coefficient of the PA radical due to reaction with NO, $k^I(T)$. The reaction time was calculated from the relative position of the injector and the flow velocity in the flow tube. High flow velocities were employed in order to reduce PA self-recombination and recombination reaction with NO_2.

The diffusion coefficient of PA at 273 K is estimated to be 225 cm^2 Torr/s using the Chapman−Enskog approach for hard spheres,[17] assuming the collision diameter of CH_3COOCH_3.[18] The optimized correlation equation formulated by Fuller, Shettler, and Giddings[17] yields an estimate of $D = 258$ cm^2 Torr/s, similar to the value suggested by Villalta et al.[19] Under the experimental conditions employed here, the correction to the rate constant due to axial diffusion[20] was less than 0.2%. Using the correction proposed by Keyser,[21] it was also verified that the error due to the radial concentration gradient is small (less than 2% for all experiments) compared with other errors associated with concentration, pressures, and other systematic errors that are included in the analysis. Therefore, no diffusion correction was applied in this study.

For each temperature, a series of measurements with different NO concentrations were taken. The second-order rate coefficient

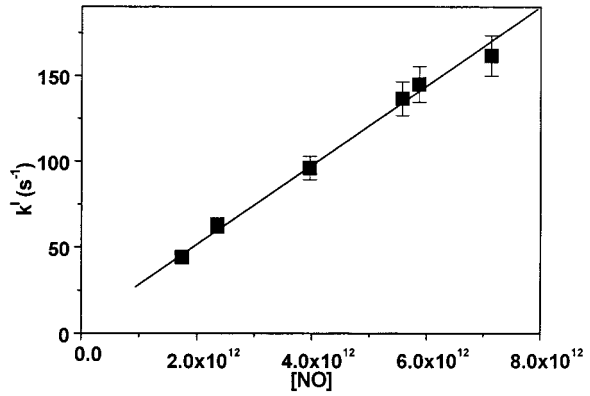

Figure 5. Plot of k^I vs [NO] for a temperature of 242 K. The straight line is a least-squares fit of the decays obtained at that temperature. The fit gives a rate coefficient of $(2.31 \pm 0.08) \times 10^{-11}$ cm^3 molecule^{-1} s^{-1}, where the error bars are at the 95% confidence level of the fit.

TABLE 1: Compilation of Measured Rate Coefficients[a]

T (K)	K (10^{-11} cm^3 molecule^{-1} s^{-1})	no. of experiments	P (Torr)	V (cm s^{-1})	[NO] ($\times 10^{12}$ cm^{-3})
218	2.51 ± 0.09	4	2.8−4.5	1935−3130	1.5−8.4
242	2.31 ± 0.08	6	3.7−4.6	2055−2635	1.7−7.1
250	2.02 ± 0.14	6	4.8	1840−1880	2.9−10.8
270	2.21 ± 0.15	6	4.6	2300−2341	3.0−7.9
295	2.00 ± 0.13	8	3.6−4.7	2400−3145	1.5−6.4
297	1.95 ± 0.18	8	4.1−5.1	2440−2930	3.1−6.4
333	1.56 ± 0.08	6	4	2760−3150	2.5−8.5
351	1.28 ± 0.10	5	4.1−4.6	2685−3015	3.6−6.1
370	1.42 ± 0.13	9	4.3	3025−3125	2.5−7.4

[a] Error is at the 95% confidence level.

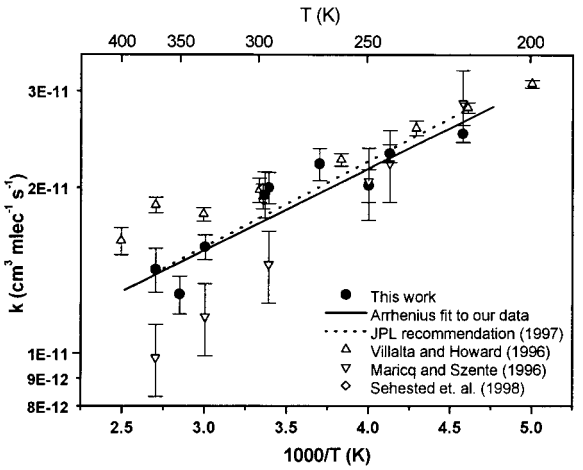

Figure 6. Arrhenius plot of the data listed in Table 1 (solid circles) and of results from Villalta et al.[4] (△), Maricq et al.[5] (▽), and Sehested et al.[6] (◇). The straight line is a nonlinear least-squares fit of our data, and the dashed line is the NASA recommended expression.

at any given temperature was obtained by plotting the first-order decay rates (k^I) vs [NO] for all runs on different experiments, at different pressures, signal intensities, and NO/He bulb concentrations (see Figure 5). The error assigned for each k^I value is the propagation of the error from the decay curve and a 7% systematic error value associated with the experimental apparatus. Table 1 shows the derived second-order rate coefficients for the PA + NO reaction. The rate coefficients measured at different temperatures are plotted vs $1/T$ to obtain an Arrhenius plot as shown in Figure 6. An Arrhenius fit to these data yields $k(T) = (6.0 \pm 1.1) \times 10^{-12} \exp\{(320 \pm 40)/T\}$ cm^3 molecule^{-1} s^{-1}. The uncertainty in the Arrhenius

preexponential coefficient incorporates a ±10% factor for possible systematic error. The room-temperature rate coefficient calculated using this expression is $k_{298} = (1.8 \pm 0.3) \times 10^{-11}$ cm^3 molecule^{-1} s^{-1}.

Discussion

PAN does not produce a peak at the parent mass. The signals observed after heating PAN may lead one to assume that the two sets of peaks, 75−46 and 59−62, are direct thermal decomposition products of the parent PAN molecule.

$$\mathrm{PAN} \rightarrow \mathrm{CH_3C(O)O_2} + \mathrm{NO_2} \quad (\Delta H \approx -30 \text{ kcal/mol}) \quad (5)$$

$$\mathrm{PAN} \rightarrow \mathrm{CH_3C(O)O} + \mathrm{NO_3} \quad (\Delta H \approx -30 \text{ kcal/mol}) \quad (6)$$

The thermal decomposition of peroxyacetyl nitrate (PAN) has been studied over the past decade.[11,22,23] It was shown that R6 is not significant[23] with an upper limit to the reaction at 345 K of $k_6 = 8 \times 10^{-5}$ s^{-1}. In comparison, the major channel for thermal decomposition of PAN, R5, has a rate constant of $k_5 \cong 0.2$ s^{-1} at the same temperature.[23] Therefore, it is inconceivable that the peak at *m*/*e* 62 is due to R6. In addition, the intensity of $CH_3C(O)O^-$ does not change due to NO addition, although such increase is expected if this mass forms from reaction R2. (The electron affinities of SF_6 and $CH_3C(O)O$ are 1.06 and 3.07 eV, respectively[24] and should enable a fast charge-transfer reaction between SF_6^- and $CH_3C(O)O$.) This also suggests that the *m*/*e* 59 peak does not arise from neutral species as well. In addition, from Figure 2 it can be observed that the anions at masses 62 and 59 are formed at temperatures lower than ∼430 K, at which PAN does not thermally dissociate. All of these observations suggest that the signals at *m*/*e* 59 and 62 arise from ion−molecule reactions of PAN with SF_6^- that yield NO_3^- and $CH_3C(O)O^-$, rather than being products of the thermal decomposition.

$$\mathrm{CH_3C(O)O_2NO_2} + \mathrm{SF_6^-} \rightarrow \mathrm{CH_3C(O)O^-} + \mathrm{NO_3} + \mathrm{SF_6} \quad (7)$$

$$\mathrm{CH_3C(O)O_2NO_2} + \mathrm{SF_6^-} \rightarrow \mathrm{CH_3C(O)O} + \mathrm{NO_3^-} + \mathrm{SF_6} \quad (8)$$

The existence of reactions R7 and R8 have also recently been suggested by Srinivasan et al. in a study on the proton affinity of PAN.[25]

The kinetic measurements reported in this study are based solely on monitoring the decrease of the $CH_3C(O)O_2^-$ signal due to the reaction with NO. No decrease in other masses was observed. Nonetheless, undetected reaction products (such as CH_3 and HO_2) can potentially influence the NO/NO_2 ratio and $CH_3C(O)O_2$ production and loss and therefore should be considered. Comprehensive reaction models are detailed by Sehested et al. and Maricq and Szente.[5,6] These chemical mechanisms, however, include many additional reactions due to excess O_2 and CO_2 in the system used for the PA formation. In the current experiments, the only source of oxygen would be from self-reactions within the injector. If methylperoxy radicals are formed, they too can react with the parent peroxyacetyl radicals. We explored the potential effect of secondary reactions by using a chemical kinetics simulation of the chemical reactions involved, assuming an initial PA concentration of 2×10^{11} cm^{-3} and a highly overestimated O_2 from self-reactions of 2×10^{10} cm^{-3}. The reactions included in the model are listed in Table 2. No significant contribution to the chemistry due to CH_3O_2 formation and subsequent PA depletion is observed. Subsequent reactions of the PA with NO_2 (either from contamination in the NO bulb or as a reaction product) are also minimal, as was also verified experimentally by monitoring the change in $CH_3C(O)O_2^-$ peak after addition of pure NO_2 into the flow.

TABLE 2: Rate Coefficients Used to Model the Conditions in the Flow Tube[a]

reaction	rate coefficient (cm^3 molecule^{-1} s^{-1})
$CH_3C(O)O_2 + NO \rightarrow CH_3C(O)O + NO_2$	1.8×10^{-11}
$CH_3C(O)O_2 + CH_3C(O)O_2 \rightarrow CH_3C(O)O + CH_3C(O)O + O_2$	2×10^{-11}
$CH_3C(O)O \rightarrow CH_3 + CO_2$	1×10^6 (S^{-1})
$CH_3 + O_2 + M \rightarrow CH_3O_2 + M$	5×10^{-14}
$CH_3O_2 + NO \rightarrow CH_3O + NO_2$	7.7×10^{-12}
$NO + NO_3 \rightarrow 2NO_2$	2.6×10^{-11}
$CH_3O + NO + M \rightarrow CH_3ONO + M$	5×10^{-14}

[a] All the rate coefficients are taken from DeMore et al.[8] and from this work.

To further validate that the 75 signal ratio represents depletion of $CH_3C(O)O_2^-$ solely due to reaction with NO, SIM scans (selected ion monitoring) were taken at the $m/e = 75$ prior to and after the addition of NO to ensure that no residual NO was influencing consecutive measurements. Shortly after NO is introduced to the flow tube, the intensity decreases but recovers to the original value on a time scale of seconds when the NO flow is stopped.

The room-temperature rate coefficient derived from the present study using the obtained Arrhenius parameters yields $k_{298} = (1.8 \pm 0.3) \times 10^{-11}$ cm^3 molecule^{-1} s^{-1}. At the low-temperature range, the rate coefficient is in good agreement with the former flow tube study.[4] The room-temperature rate coefficient also agrees with the results of Sehested et al.[6] There is disagreement between the current results and those of Mariq and Szente[5] largely at $T > 250$ K. The sources of this discrepancy are not clear, but they may originate from the higher concentrations and the less direct measurement technique used in the Mariq and Szente study. Our measurement is in excellent agreement with the current NASA-JPL compilation[8] over the whole temperature range. Therefore, we recommend to use this rate expression for atmospheric chemical modeling.

The slight negative temperature dependence of the $CH_3C(O)O_2 + NO$ reaction observed here is expected since this type of behavior is common for fast radical−radical reactions. Similar results were obtained for other peroxy radical reactions with NO.[4,13,14,16,24] Qualitatively, this type of temperature dependence is explained by the formation of a reaction intermediate.

$$\mathrm{RO_2} + \mathrm{NO} \rightarrow [\mathrm{RO_2 \cdot NO}]^* \rightarrow \mathrm{RO} + \mathrm{NO_2} \quad (9)$$

This reaction mechanism was proposed before for reactions of peroxy radicals with NO[15,24] and was treated in terms of transition state theory.[26]

The rate constants measured in this study are very similar to the results of a flow tube study of the analogous reaction $CH_2{=}C(CH_3)C(O)O_2 + NO$,[16] suggesting that the rate coefficients of these reactions are mainly determined by the $C(O)O_2$ functional group and are not very sensitive to the character of the organic moiety. This conclusion is similar to the conclusions about the reactions of C_3-C_5 hydrocarbon peroxy radicals with NO, which also seem to be insensitive to the character of the hydrocarbon backbone.[15]

Atmospheric Implications. In the lower troposphere, the lifetime of PAN against thermal decomposition is a few minutes. Therefore, PAN is expected to be in equilibrium with NO_2 and peroxy radicals.[27] The lifetime of PAN, under these conditions

is determined by the rates of reactions R1 and R2, according to the equation

$$\tau = \left(1 + \frac{k_1[NO_2]}{k_2[NO]}\right)(k_{-1})^{-1}$$

where k_{-1} is the rate coefficient for PAN thermal decomposition. The ratio k_1/k_2 is, therefore, an important quantity for atmospheric modeling of PAN in the atmosphere. For example, apparent underprediction of the PAN production rate is evident in the model analysis of the ROSE (rural oxidants in the southern environment) measurements.[27] In this study, the measured PAN concentrations were used. It was found that the PAN production (R1) rate was slower than its loss rate (PAN thermal decomposition and OH reaction) so that PAN decomposition represented a net radical source. Two possible reasons for this discrepancy were given: (1) the model mechanism was not accounting for some PAN sources, perhaps from isoprene oxidation, or (2) the boundary layer was not well enough mixed early and late in the day and free tropospheric levels of PAN, which were not in steady state at boundary layer temperature, were measured. However, a low NO_2 + PA rate constant (or a too high PAN decomposition rate) is also consistent with these results. Such discrepancies call for a better determination of the rate coefficients used in the modeling of PAN chemistry.

In a recent study, the ratio $k_2/k_1 = 2.07 \pm 0.21$ was directly determined using SF_6 and CO_2 as bath gases.[6] On the basis of this measurement, as well as previous determinations of this ratio, Sehested et al. suggest to use an average value of $k_2/k_1 = 2.17 \pm 0.33$ in atmospheric chemistry models.[6] Our determination of k_2, combined with this value, allows indirect determination of k_1 and comparison with its recommended values by the JPL-NASA[8] and IUPAC[28] evaluation panels. There is a difference of 20−30% in the value of k_1 calculated in this manner compared to its recommended values between 250 and 300 K. This difference points to inconsistencies within the database of the NO_2 and NO rate coefficients with the PA radical used for atmospheric chemistry modeling and calls for more laboratory and field work that will resolve this issue.

Conclusions

The rate coefficient of the peroxyacetyl radical with NO was directly measured by flow tube and chemical ionization mass spectrometry between 218 and 370 K and 2−5 Torr. The temperature-dependent expression for the rate coefficient was determined to be $k(T) = (6.0 \pm 1.1) \times 10^{-12} \exp\{(320 \pm 40)/T\}$ cm^3 molecule^{-1} s^{-1}. The 298 K rate constant is $k_{298} = (1.8 \pm 0.3) \times 10^{-11}$ cm^3 molecule^{-1} s^{-1}. These results are used to remove some of the discrepancies between two previous direct measurements of this reaction. This measurement is also used to derive the rate coefficient of the PA + NO_2 reaction.

Acknowledgment. Yinon Rudich is the incumbent of the William Z. and Eda Bess Novick career development chair. This work was partially funded by the Israeli Science Foundation founded by the Israeli Academy of Sciences and Humanities and the MINERVA Science Foundation. Tamar Moise appreciates the financial support of the Sussman Family Center for Environmental Studies for a fellowship for participating in the European Research Course on Atmospheres.

References and Notes

(1) Cox, R. A.; Roffey, M. J. *Environ. Sci. Technol.* **1977**, *11*, 900.
(2) Kirchner, F.; Zabel, F.; Becker, K. H. *Ber. Bunsen Phys. Chem.* **1990**, *94*, 1379.
(3) Hendry, D. G.; Kenley, R. A. *J. Am. Chem. Soc.* **1977**, *99*, 3198.
(4) Villalta, P. W.; Howard, C. J. *J. Phys. Chem.* **1996**, *100*, 13624.
(5) Maricq, M. M.; Szente, J. J. *J. Phys. Chem.* **1996**, *100*, 12380.
(6) Sehested, J.; Christensen, L. K.; Mogelberg, T.; Nielsen, O. J.; Wallington, T. J.; Guschin, A.; Orlando, J. J.; Tyndall, G. S. *J. Phys. Chem. A* **1998**, *102*, 1779.
(7) Seefeld, S.; Kinnison, D. J.; Kerr, J. A. *J. Phys. Chem. A* **1997**, *101*, 55.
(8) DeMore, W. B.; Sander, S. P.; Golden, D. M.; Hampson, R. F.; Kurylo, M. J.; Howard, C. J.; Ravishankara, A. R.; Kolb, C. E.; Molina, M. J. *Chemical kinetics and photochemical data for use in stratospheric modeling*, evaluation 11; JPL publication 97-4; JPL, 1997.
(9) Talukdar, R. K.; Burkholder, J. B.; Schmoltner, A. M.; Roberts, J. M.; Wilson, R. R.; Ravishankara, A. R. *J. Geophys. Res. Atmos.* **1995**, *100*, 14163.
(10) Roberts, J. M. *Atmos. Environ.* **1990**, *24A*, 243.
(11) Roberts, J. M.; Bertman, S. B. *Int. J. Chem. Kinet.* **1992**, *24*, 297.
(12) Gaffney, J. S.; Fajer, R.; Senum, G. I. *Atmos. Environ.* **1984**, *18*, 215.
(13) Eberhard, J.; Villalta, P. W.; Howard, C. J. *J. Phys. Chem.* **1996**, *100*, 993.
(14) Eberhard, J.; Howard, C. J. *Int. J. Chem. Kinet.* **1996**, *28*, 731.
(15) Eberhard, J.; Howard, C. J. *J. Phys. Chem. A* **1997**, *101*, 3360.
(16) deGouw, J. A.; Howard, C. J. *J. Phys. Chem. A* **1997**, *101*, 8662.
(17) Fuller, E. N.; Schettler, P. D.; Giddings, J. C. *Indust. Eng. Chem.* **1966**, *58*, 19.
(18) Monchick, L.; Mason, E. A. *J. Chem. Phys.* **1961**, *35*, 1676.
(19) Villalta, P. W.; Lovejoy, E. R.; Hanson, D. R. *Geophys. Res. Lett.* **1996**, *23*, 1765.
(20) Howard, C. J. *J. Phys. Chem.* **1979**, *83*, 3.
(21) Keyser, L. F. *J. Phys. Chem.* **1984**, *88*, 4750.
(22) Grosjean, D.; Grosjean, E.; Williams, E. L., II *J. Air Waste Manage. Assoc.* **1994**, *44*, 391.
(23) Orlando, J. J.; Tyndall, G. S.; Calvert, J. G. *Atmos. Environ.* **1992**, *26*, 3111.
(24) Villalta, P. W.; Huey, L. G.; Howard, C. J. *J. Phys. Chem.* **1995**, *99*, 12829.
(25) Srinivasan, N.; Cooks, R. G.; Shepson, P. B. *Rapid Commun. Mass Spectrom.* **1998**, *12*, 328.
(26) Golden, D. M. *J. Phys. Chem.* **1979**, *83*, 108.
(27) Frost, G. J.; Trainer, M.; Allwine, G.; Buhr, M. P.; Calvert, J. G.; Cantrell, C. A.; Fehsenfeld, F. C.; Goldan, P. D.; Herwehe, J.; Hubler, G.; Kuster, W. C.; Martin, R.; McMillen, R. T.; Montzka, S. A.; Norton, R. B.; Parrish, D. D.; Ridley, B. A.; Shetter, R. E.; Walega, J. G.; Watkins, B. A.; Westberg, H. H.; Williams, E. J. *J. Geophys. Res.* **1998**, *103*, 22491.
(28) Atkinson, R.; Baulch, D. L.; Cox, R. A.; Hampson, R. F.; Kerr, J. A.; Rossi, M. J.; Troe, J. *J. Phys. Chem. Ref. Data* **1997**, *26*, 521.